

Parameter estimation from gravitational waves generated by non-spinning binary black holes with laser interferometers: beyond the Fisher information.

S. Vitale^{1,2,3} and M. Zanolin¹

¹*Embry-Riddle Aeronautical University, 3700 Willow Creek Road, Prescott, AZ, 86301, USA*

²*LPTMC, Université Pierre-et-Marie-Curie - 4, Place Jussieu, 75005 Paris, France*

³*Nikhef, Science Park 105, 1098 XG Amsterdam, The Netherlands*

In this paper we apply to gravitational waves from non-spinning binary systems a recently introduced frequentist methodology to calculate analytically the error for a maximum likelihood estimate (MLE) of physical parameters. While existing literature focuses on using the Cramer Rao Lower bound (CRLB) and Monte Carlo simulations, we use a power expansion of the bias and covariance in inverse powers of the signal to noise ratio. The use of higher order derivatives of the likelihood function in the expansions makes the prediction also sensitive to the secondary lobes of the MLE probability distribution. We discuss conditions for validity of the CRLB and predict new features in regions of the parameter space currently not explored. For example, we see how the bias can become the most important contributor to the parameters' errors for high mass systems ($200M_{\odot}$ and above).

I. INTRODUCTION

Coalescing black holes binaries (BBH) are among the most promising sources of gravitational waves (GW) transients [1]. Observations strongly indicate the existence of stellar-mass BHs ($3-10 M_{\odot}$) [4] and super massive black holes ($10^4 - 10^{10} M_{\odot}$) ([5],[6]), also suggesting the possibility of intermediate BHs ([7]). Observations and models also point to the formation of binary BH systems (BBH) ([8],[9],[10],[11],[12],[13],[14],[15],[16]). The chances of observation of BBH GWs in the next few years are promising given the advanced generation of laser interferometers currently under construction ([2],[3]) and recent advances in modeling the BBH waveforms. In fact, even if the inspiral and ringdown phases of the life of a binary system are well understood (the inspiral GW can be computed using Post-Newtonian approximations ([24]), while the GW for the ringdown phase can be obtained with black hole perturbation theories) only recently numerical breakthroughs in numerical relativity made compute GWs from the merger phase possible ([25], [26], [27], [28], [29], [30], [31], [32]). The GW community is actively preparing for detection and parameter estimation opportunities in GWs from BBHs [21] and plans are shaping up to explore all the interesting regions of the parameter space. P. Ajith and collaborators ([38]) have proposed a template bank for the waveform coming from a coalescing binary system, made of non-spinning masses, that takes into account the inspiral merger and ringdown stages of the binary's life (IMR). IMR waveforms are obtained by tuning numerical parameters of a phenomenological wave (see [38]) to a set of numerical calculations performed in the full GR. Other attempts to produce analytical approximations have been developed in more recent times, like the effective one body model (EOB) proposed in [18], that

was used in the fifth LIGO run S5. The most accurate EOB model in the literature is described in ([19], [17]). The discrepancies between different analytical approximations to numerical relativity waveforms are described in [20] and show for example that the amplitude of the IMR waveforms can be up to 20% different from the EOB ones. This means that a binary at a given distance could produce a signal to noise ratio (SNR) at receiver up to 20% different from the one expected using IMR waveforms.

This paper discusses the estimation accuracy of BBH physical parameters which can be obtained with advanced configuration laser interferometers and IMR waveforms. Existing literature [40] predicts the errors with approaches that have some intrinsic limitations: (a) with the square root of the inverse of the Fisher information matrix elements (commonly named Cramer Rao Lower Bound (CRLB), [23]) that only takes into account the curvature of the likelihood function around the true value of the parameters. The CRLB is known to underestimate the error in low signal to noise ratio (SNR) ([34], [35], [36]) and is the lowest possible uncertainty for unbiased estimators, or (b) perform simplified Monte Carlo simulations. In the MC simulations [40] η is enforced to values ≤ 0.25 and the simulations do not explore the secondary peaks of the likelihood function.

A recent paper, [22], from the authors, studies the problem of MLE errors from GWs from the inspiral phase of binary systems with asymptotic expansions for the covariance and the bias in terms of power series in the inverse of the SNR. The first order of the covariance series is the inverse of the Fisher information matrix. The second order is a more complicated expression that depends on the secondary maximum of the probability distribution because it contains higher order derivatives of the likelihood function (up to the fourth). The first two orders of the covariance and

bias expansion are a better tool than the CRLB to estimate the errors and allow the determination of necessary conditions for the validity of the CRLB (for example by requiring the second order to be much smaller than the first). These conditions allow predictions to be made on the interferometers' capability to estimate parameters in different regions of the parameter space. We show that the variation of the errors in the parameter space is more complicated than as predicted solely by the CRLB and that the existence of minima for particular values of the masses can happen even without including the merger phase. We also predict that the bias can become the most important contributor to the parameters' errors for high mass systems ($200M_\odot$ and above), due to the nonlinear dependence of the signal on the parameters (these regions of the parameter space are not yet explored).

In section II we define the data model, the MLE, the statistical errors and how to compute the asymptotic expansions. In section III we give the analytical expression for the IMR GW for BBHs, and the noise spectra for the advanced configurations of LIGO and Virgo. In section IV the results are described.

II. STATISTICAL MODEL

We model the output $x(t)$ of a GW detector as the sum of the GW signal $h(t, \theta^\mu)$, that depend on the vector of unknown parameters θ^μ , and a Gaussian stationary noise $w(t)$ with zero mean, $E[w(t)] = 0$, with $E[A]$ denoting the mean of A over the ensemble

$$x(t) = h(t, \theta^\mu) + w(t) \quad (2.1)$$

If one expects the wave to have a known analytical form it is possible to perform an estimation of the parameters by filtering detector data with a bank of waveform templates. In Gaussian noise, this is a maximum likelihood estimation.

Given the Fourier transform for a function $h(t)$ as $h(f) \equiv \int dt e^{-2\pi i f t} h(t)$, the expectation of the product

of two functions can be written like a scalar product

$$\langle u(f) | v(f) \rangle \equiv 2 \int_{f_{low}}^{f_{cut}} df \frac{u(f)v(f)^* + u(f)^*v(f)}{S_h(f)} \quad (2.2)$$

where the range of integration depends on the antenna properties and on the theoretical model for the binary system, and where we introduced the *one sided noise spectral density*, $S_h(f)$ defined by $E[w(f)w(f')] = \frac{1}{2}S_h(f)\delta(f-f')$. The SNR corresponding to the optimal filter is defined as

$$\rho^2 \equiv \langle h(f), h(f) \rangle = 4 \int_{f_{low}}^{f_{cut}} df \frac{|h(f)|^2}{S_h(f)} \quad (2.3)$$

Once the values of the parameters are estimated using matched filters, the accuracy can be evaluated with the square root of the mean squared error (MSE) for the j -th parameter:

$$\begin{aligned} MSE_{\vartheta^j} &\equiv E \left[\left(\hat{\vartheta}^j - E(\hat{\vartheta}^j) \right)^2 \right] + \left(E \left[\hat{\vartheta}^j - \vartheta^j \right] \right)^2 \\ &\equiv \sigma_{\vartheta^j}^2 + b_{\vartheta^j}^2 \end{aligned} \quad (2.4)$$

For large SNRs one can use the CRLB to obtain a lower bound for the error of the j -th parameter $MSE_{\vartheta^j} \geq [i^{-1}]_{jj}$, where i is the *Fisher Information* matrix, whose (jk) element can be written as a scalar product of signal's first derivatives $i_{jk} \equiv \langle h(f)_j, h(f)_k \rangle$ where $h(f)_j \equiv \frac{\partial h(f)}{\partial \vartheta^j}$. The above notation allows for more concise formulae: $\langle h_{ab\dots m}, h_{no\dots z} \rangle \equiv \langle ab\dots m | no\dots p \rangle$, where the f dependence is not explicitly shown. The scalar product is the one defined in eq. 2.2. In [22] expansions for both the covariance and the bias like power series on $1/\rho$ are given as:

$$\sigma_{\vartheta^i}^2 = \frac{S_1^2}{\rho^2} + \frac{S_2^2}{\rho^4} + \dots = \sigma_{\vartheta^i}^2[1] + \sigma_{\vartheta^i}^2[2] + \dots \quad (2.5)$$

$$b_{\vartheta^i} = \frac{B_1}{\rho} + \frac{B_2}{\rho^2} + \dots = b_{\vartheta^i}[1] + b_{\vartheta^i}[2] + \dots \quad (2.6)$$

where the first order covariance is the CRLB, and the second order can be written as:

$$\begin{aligned} \sigma_{\vartheta^j}^2[2] &= i^{jm} i^{jn} i^{pq} (v_{nmpq} + 3\langle nq | pm \rangle + 2v_{nmp,q} + v_{mpq,n}) + \\ &+ i^{jm} i^{jn} i^{pz} i^{qt} \left(v_{npm} v_{qzt} + \frac{5}{2} v_{npq} v_{mzt} + 2v_{qz,n} v_{mtp} + 2v_{qp,z} v_{nmt} + \right. \\ &\left. + 6v_{mqp} v_{nt,z} + v_{pqz} v_{nt,m} + 2v_{mq,z} v_{pt,n} + 2v_{pt,z} v_{mq,n} + v_{mz,t} v_{nq,p} \right) \end{aligned} \quad (2.7)$$

where

$$v_{a_1 \dots a_s, b_1 \dots b_p, \dots, z_1 \dots z_q} = E [h_{a_1 \dots a_s} h_{b_1 \dots b_p} \dots h_{z_1 \dots z_q}]$$

are expectations of product of the signal derivatives in the time domain. For example: $v_{abc,d} = E[h_{ab} h_c h_d]$.

Using some algebra, the following explicit expressions can be given, in the frequency space:

$$v_{a,b} = -v_{ab} = i_{ab} = \langle a | b \rangle \quad (2.8)$$

$$v_{ab,c} = \langle ab | c \rangle \quad (2.9)$$

$$v_{abc,d} = \langle abc | d \rangle \quad (2.10)$$

$$v_{abc} = -\langle ab | c \rangle - \langle ac | b \rangle - \langle bc | a \rangle \quad (2.11)$$

$$v_{ab,cd} = \langle ab | cd \rangle + \langle a | b \rangle \langle c | d \rangle \quad (2.12)$$

$$v_{abcd} = -\langle ab | cd \rangle - \langle ac | bd \rangle - \langle ad | bc \rangle - \langle abc | d \rangle - \langle abd | c \rangle - \langle acd | b \rangle - \langle bcd | a \rangle$$

$$v_{ab,c,d} = -\langle a | b \rangle \langle c | d \rangle = -i_{ab} i_{cd} \quad (2.13)$$

$$v_{abc,de} = \langle abc | de \rangle - i_{de} v_{abc} \quad (2.14)$$

$$v_{abcd,e} = \langle abcd | e \rangle \quad (2.15)$$

$$v_{abc,d,e} = i_{de} v_{abc} \quad (2.16)$$

$$v_{ab,cd,e} = -i_{ab} v_{cd,e} - i_{cd} v_{ab,e} \quad (2.17)$$

$$\begin{aligned} v_{abcde} = & -\langle abcd | e \rangle - \langle abc | de \rangle - \langle abde | c \rangle - \langle acde | b \rangle \\ & -\langle bcde | a \rangle - \langle abc | de \rangle - \langle abd | ce \rangle - \langle acd | be \rangle \\ & -\langle bcd | ae \rangle - \langle abc | cd \rangle - \langle ace | bd \rangle - \langle bce | ad \rangle \\ & -\langle ade | bc \rangle - \langle bce | ac \rangle - \langle cde | ba \rangle \end{aligned} \quad (2.18)$$

Where i_{jk} is the Fisher information matrix.

The reason for the presence of $3\langle nq | pm \rangle$ in (2.7) is that this expression is a simplified version of the eq. 2.4 we gave in [22], in which some of the v have been replaced with their values in terms of scalar product. This allows for slightly shorter expression. The same kind of simplifications can be performed on the first and second orders of the bias, that have a final form shorter than that presented in [22]:

$$b_{\vartheta^r}[1] = \frac{1}{2} i^{ra} i^{bc} (v_{abc} + 2v_{c,ab}) \quad (2.19)$$

$$\begin{aligned} b_{\vartheta^m}[2] = & \frac{i^{ma} i^{bd} i^{ce}}{8} [v_{abcde} + 4\langle ac | bde \rangle + 8\langle de | abc \rangle + 4v_{abc,e,d}] \\ & + \frac{i^{ma} i^{bc} i^{df} i^{eg}}{4} \left[(2v_{afed} v_{gb,c} + 2v_{bedf} v_{ac,g} + 4v_{abed} v_{gf,c}) + (v_{afed} v_{gcb} + \right. \\ & + 2v_{abed} v_{gcf} + 2v_{dbeg} v_{acf}) + (2v_{aed} \langle gb | fc \rangle + 4v_{acf} \langle dg | eb \rangle + 4v_{bed} \langle ac | gf \rangle \\ & + 2v_{fcb} \langle ag | ed \rangle) + (4v_{afe,g} v_{db,c} + 4v_{afe,c} v_{db,g} + 4v_{dbe,g} v_{af,c}) + (2v_{abe,g} v_{cdf} \\ & + 4v_{dbe,g} v_{acf} + 4v_{abe,f} v_{cdg} + 2v_{dge,b} v_{acf}) + (4\langle ag | fc \rangle v_{ed,b} + 4\langle ed | fc \rangle v_{ag,b} \\ & \left. + 4\langle ag | ed \rangle v_{fc,b}) \right] \\ & + \frac{i^{ma} i^{bc} i^{de} i^{fg} i^{ti}}{8} [v_{adf} (v_{ebc} v_{gti} + 2v_{etc} v_{gbi} + 4v_{gbe} v_{tci} + 8v_{gbt} v_{eci} + 2v_{ebc} v_{gt,i} \\ & + 4v_{etc} v_{gb,i} + 2v_{gti} v_{eb,c} + 4v_{gtc} v_{eb,i} + 8v_{gbi} v_{ce,i} + 8v_{gbt} v_{ci,e} + 8v_{gbe} v_{ct,i} + 8v_{cte} v_{gb,i} \\ & + 4v_{cti} v_{gb,e} + 4v_{gt,i} v_{eb,c} + 4v_{eb,i} v_{gt,c} + 8v_{gt,b} v_{ic,e} + 8v_{gt,e} v_{ic,b} + 4v_{bet} v_{g,c,i}) \\ & + v_{dci} (8v_{bgt} v_{ae,f} + 4v_{bgf} v_{ae,t} + 8v_{ae,t} v_{bg,f} + 8v_{ae,f} v_{bg,t} + 8v_{af,b} v_{ge,t})] \end{aligned} \quad (2.20)$$

III. THE IMR WAVEFORM

IMR waveforms were obtained by tuning numerical parameters of a phenomenological wave to a set of numerical calculations performed in the full GR, [38]. Afterwards, the faithfulness of the IMR waves has been improved ([39], [40], [41]) and they have been used for the purpose of parameter estimation. In this work we follow the model presented in [40]. The IMR waveform is written directly in the Fourier space

(while the EOB are calculated in the time domain), as a piecewise function with a part for the inspiral, one for the merger, and another for the ringdown phase. Explicitly, we write the GW in the Fourier space as:

$$h(f) = A_{eff}(f) e^{i\Psi_{eff}(f)} \quad (3.1)$$

where the phase and the amplitude are expressed as:

$$A_{eff}(f) \equiv \mathcal{A} f_{merg}^{-7/6} \begin{cases} (f/f_{merg})^{-7/6} & \text{if } f < f_{merg} \\ (f/f_{merg})^{-2/3} & \text{if } f_{merg} \leq f < f_{ring} \\ \omega \mathcal{L}(f, f_{ring}, \sigma) & \text{if } f_{ring} \leq f < f_{cut} \end{cases} \quad (3.2)$$

$$\Psi_{eff}(f) \equiv 2\pi f t_a + \phi_a + \frac{1}{\eta} \sum_{k \in \{0,2,3,4,6\}} (x_k \eta^2 + y_k \eta + z_k) (\pi M f)^{\frac{k-5}{3}}. \quad (3.3)$$

We have defined:

$$\omega \equiv \frac{\pi \sigma}{2} \left(\frac{f_{ring}}{f_{merg}} \right)^{-\frac{2}{3}} \quad (3.4)$$

$$\mathcal{L}(f, f_{ring}, \sigma) \equiv \frac{1}{2\pi} \frac{\sigma}{(f - f_{ring})^2 + \sigma^2/4} \quad (3.5)$$

The phenomenological parameters $f_{merg}, f_{ring}, \sigma, f_{cut}$ depends on the total and symmetrized mass, via the following expressions:

$$f_i \equiv \frac{a_i \eta^2 + b_i \eta + c_i}{\pi M}$$

with $i = [merg, ring, \sigma, cut]$ (for the values of the numerical coefficients a, b, c, x, y, z see [39]). They represent the frequency at which the system passes from its inspiral phase to the merger (f_{merg}), from the merger to the ringdown (f_{ring}), and the frequency for which the signal ceases to be described by this model (f_{cut} , this is also the upper limit of the integrals (2.2)). This signal depends on five physical parameters ($\mathcal{A}, t_a, \phi_a, M, \eta$): (I) \mathcal{A} is the amplitude of the wave. It can be expressed as $\mathcal{A} = \frac{M^{5/6}}{d \pi^{2/3}} \sqrt{\frac{5\eta}{24}}$, where d is the effective distance of the binary. (II) t_a is the arrival time of the GW at the detector. (III) ϕ_a is the arrival phase, i.e. the phase of the signal at the time t_a . (IV) M is the total mass of the binary. (V) η is the symmetrized mass ratio: $\eta \equiv m_1 m_2 / M^2$. Sometime the chirp mass is used in the literature, instead of the total mass. They are related by $M_{chirp} = \eta^{\frac{3}{5}} M$.

If one considers the merger and ringdown phase too, the amplitude is not uncoupled from the other parameters. One can not work in the simplified four-dimensional parameter space obtained by treating the amplitude as a known constant ([22], [43],[44]), and the full five dimensional space must be considered.

We perform the calculations using either the design advanced Ligo (AdvLIGO) or advanced Virgo (AdvVirgo) noises, as they are given in [40]. The Adv

Ligo one sided noise spectral density is written as:

$$S_h(f) = S_0 \left[x^{-4.14} - 5x^{-2} + 111 \frac{1 - x^2 + x^4/2}{1 + x^2/2} \right], \quad f \geq f_{low}$$

$$S_h(f) = \infty, \quad f \leq f_{low} \quad (3.6)$$

where the lower frequency cutoff value is $f_{low} = 10\text{Hz}$, $x \equiv \frac{f}{f_0}$, $f_0 = 215\text{Hz}$, and $S_0 = 10^{-49}\text{Hz}^{-1}$. While for the AdvVirgo:

$$S_h(f) = S_0 \left[2.67 \cdot 10^{-7} x^{-5.6} + 0.68 e^{-0.73(\ln x)^2} x^{5.34} \right. \\ \left. + 0.59 e^{(\ln x)^2 [-3.2 - 1.08 \ln x - 0.13(\ln x)^2]} x^{-4.1} + \right. \\ \left. + 0.68 e^{-0.73(\ln x)^2} x^{5.34} \right], \quad f \geq f_{low}$$

$$S_h(f) = \infty, \quad f \leq f_{low} \quad (3.7)$$

where the lower frequency cutoff value is chosen to be $f_{low} = 10\text{Hz}$, $x \equiv \frac{f}{f_0}$, $f_0 = 720\text{Hz}$, and $S_0 = 10^{-47}\text{Hz}^{-1}$. Fig. 1 shows the value of $\sqrt{S_h(f)}$ for both detectors.

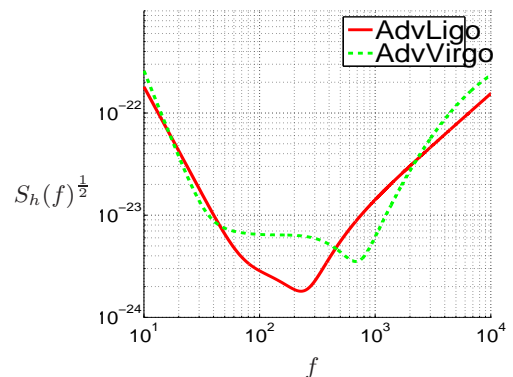


Figure 1. Power spectral densities for AdvLigo (continuous line) and AdvVirgo (dashed line)

IV. RESULTS

To be able to compare our results with those of [40], we consider $\eta = 0.16, 0.2222, 0.25$ and $M = 20, 100, 200M_\odot$. Tables 1 and 2 show the values of the first two orders of the covariance and bias for SNR=10. For each value of η and M_\odot the error estimation for t_a, ϕ_a , total mass and symmetrized mass ratio η are presented.

		$M = 200M_{\odot}$				$M = 100M_{\odot}$				$M = 20M_{\odot}$			
		$\sigma[1]$	$\sigma[2]$	$b[1]$	$b[2]$	$\sigma[1]$	$\sigma[2]$	$b[1]$	$b[2]$	$\sigma[1]$	$\sigma[2]$	$b[1]$	$b[2]$
$\eta = 0.25$	Δt	9.47	12.5	-0.45	-1.04	3.54	2.92	-0.10	0.07	0.22	0.20	$-6.6 \cdot 10^{-3}$	$-8.9 \cdot 10^{-3}$
	$\Delta \phi$	40.7	59.7	-7.85	-18.0	24.2	21.6	-2.27	-0.98	9.98	11.0	-0.42	-0.57
	$\Delta M[\%]$	6.02	9.60	0.82	1.87	2.61	2.12	$-2.24 \cdot 10^{-4}$	$-2.92 \cdot 10^{-2}$	1.38	1.44	$5.34 \cdot 10^{-3}$	$1.25 \cdot 10^{-2}$
	$\Delta \eta[\%]$	11.3	16.4	0.81	1.26	6.53	5.82	0.37	0.58	2.58	2.88	0.04	$3.64 \cdot 10^{-2}$
$\eta = 0.22$	Δt	12.0	16.3	-0.74	-1.35	4.33	3.73	-0.16	$3.79 \cdot 10^{-2}$	0.23	0.22	$-6.14 \cdot 10^{-3}$	$-8.24 \cdot 10^{-3}$
	$\Delta \phi$	63.3	94.7	-9.69	-21.6	36.5	33.9	-2.70	-1.1	13.0	14.8	-0.36	-0.49
	$\Delta M[\%]$	5.10	8.21	0.74	1.93	2.62	1.88	$9.63 \cdot 10^{-3}$	$-3.57 \cdot 10^{-2}$	1.27	1.37	$4.52 \cdot 10^{-3}$	$0.70 \cdot 10^{-2}$
	$\Delta \eta[\%]$	12.1	18.0	0.84	1.77	6.87	6.35	0.34	0.51	2.36	2.72	$3.38 \cdot 10^{-2}$	$4.03 \cdot 10^{-2}$
$\eta = 0.16$	Δt	21.8	30.0	-2.12	-3.17	7.04	6.65	-0.31	-1.04	0.25	0.26	$-4.93 \cdot 10^{-3}$	$-5.79 \cdot 10^{-3}$
	$\Delta \phi$	143	213	-18.0	-33.2	77.0	77.7	-3.75	-2.26	19.2	22.4	-3.76	-0.25
	$\Delta M[\%]$	3.07	4.21	0.48	1.26	2.75	1.70	$1.27 \cdot 10^{-3}$	$-4.84 \cdot 10^{-2}$	0.99	1.10	$2.19 \cdot 10^{-3}$	$-1.23 \cdot 10^{-3}$
	$\Delta \eta[\%]$	14.2	20.8	0.85	2.37	7.53	7.58	0.37	0.52	1.84	2.15	0.02	$3.57 \cdot 10^{-2}$

Figure 2. The errors in an Advanced Ligo detector (table above) and Advanced Virgo (below). $\sigma[1]$ and $\sigma[2]$ are the first (the usual CRLB) and second order in the variance expansion; while $b[1]$ and $b[2]$ are the first and second order of the bias (see 2.5 and 2.6). The time errors are in milliseconds, the phase errors are in radians, while the errors in the mass parameters are in percent. The SNR is equal to 10

		$M = 200M_{\odot}$				$M = 100M_{\odot}$				$M = 20M_{\odot}$			
		$\sigma[1]$	$\sigma[2]$	$b[1]$	$b[2]$	$\sigma[1]$	$\sigma[2]$	$b[1]$	$b[2]$	$\sigma[1]$	$\sigma[2]$	$b[1]$	$b[2]$
$\eta = 0.25$	Δt	10.8	11.0	-0.45	-0.17	5.69	6.30	-0.15	1.39	0.17	0.13	$-2.64 \cdot 10^{-3}$	$-2.06 \cdot 10^{-3}$
	$\Delta \phi$	42.7	49.9	-8.04	-9.37	38.9	43.28	-5.04	4.40	7.22	5.38	-0.19	-0.14
	$\Delta M[\%]$	5.58	7.07	0.55	0.64	3.85	3.89	-0.14	-1.25	0.99	0.71	$-7.04 \cdot 10^{-5}$	$3.37 \cdot 10^{-3}$
	$\Delta \eta[\%]$	11.7	12.9	1.00	1.30	10.4	11.8	1.14	4.28	1.86	1.40	$2.64 \cdot 10^{-2}$	$8.05 \cdot 10^{-3}$
$\eta = 0.22$	Δt	13.8	15.5	-0.85	-0.64	6.47	6.74	-0.19	1.14	0.18	0.14	$-2.35 \cdot 10^{-3}$	$-1.82 \cdot 10^{-3}$
	$\Delta \phi$	68.3	84.56	-10.69	-14.15	54.6	57.4	-4.58	6.18	9.37	7.26	-0.16	-0.12
	$\Delta M[\%]$	4.92	6.46	0.56	0.88	3.78	3.52	-0.13	-0.93	0.91	0.68	$-0.55 \cdot 10^{-3}$	$0.17 \cdot 10^{-2}$
	$\Delta \eta[\%]$	13.0	15.4	1.05	1.66	10.3	10.9	1.04	3.26	1.70	1.33	$2.29 \cdot 10^{-2}$	$9.89 \cdot 10^{-3}$
$\eta = 0.16$	Δt	25.6	31.7	-2.50	-2.05	8.06	7.07	-0.19	0.25	0.21	0.17	$-1.80 \cdot 10^{-3}$	$-1.16 \cdot 10^{-3}$
	$\Delta \phi$	162	217	-21.1	-26.1	89.6	80.0	-2.54	2.04	13.9	11.1	$-8.36 \cdot 10^{-2}$	$-5.63 \cdot 10^{-2}$
	$\Delta M[\%]$	3.50	3.97	0.39	0.77	3.23	2.31	-0.10	-0.24	0.72	0.55	$-7.86 \cdot 10^{-4}$	$-4.74 \cdot 10^{-4}$
	$\Delta \eta[\%]$	16.0	20.7	1.27	3.05	8.74	8.00	0.74	1.00	1.33	1.06	$1.47 \cdot 10^{-2}$	$9.23 \cdot 10^{-3}$

The CRLB consistently underestimate the error at this SNR. The errors for different values of the SNR ρ can be obtained by multiplying the first orders for $10/\rho$ and the second orders by $100/\rho^2$ (and multiplying for 10 and 100 gives S_1^2 and S_2^2). A necessary condition for the validity of the CRLB can also be obtained as:

$$\frac{S_2^2}{S_1^2 * \rho^2} < 1 \quad (4.1)$$

where the $<$ sign can be replaced by \ll depending on the accuracy needs. Using the data in the tables above, we can plot the errors against the SNR, for

fixed values of the total mass M and the mass ratio η . For example Fig. 3 shows the first order variance for the arrival time estimation, and the total variance (first plus second order) for an equal masses system of total mass $M = 200M_{\odot}$. It is clearly visible for which SNR the CRLB ceases to be faithful.

Another useful application is the calculation of the CRLB and second order variance for systems having mass and mass-ratio within a chosen range, building then a grid of results that clearly show for what systems the errors are smaller. We have done that for $M = 4M_{\odot}..200M_{\odot}$ and $\eta = 0.10..0.25$. In Fig. 4 we

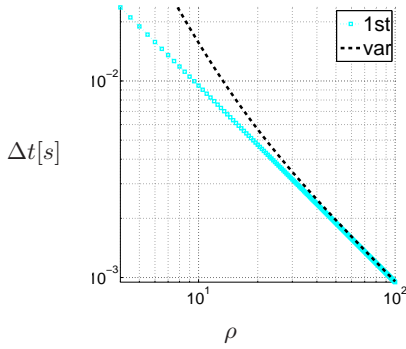


Figure 3. The error in the estimation of the arrival time for a system with $M = 200M_{\odot}$ and $\eta = 0.25$. The dot-diamonds line is the first order variance (CRLB) while the dashed line is the total variance. The bias is not shown, being negligible.

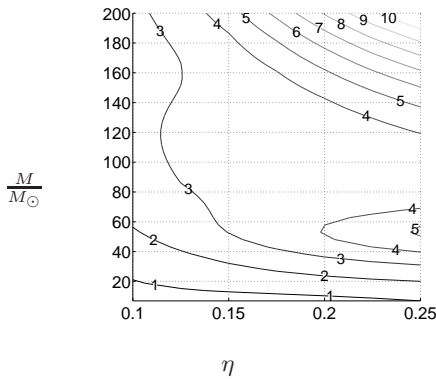


Figure 4. The percent error on the total mass estimation (first plus second order) as a function of the total mass and symmetrized mass ratio. The systems have a fixed SNR, $\rho = 10$, and the AdvLigo noise is used. This plot does not depend on the values of t_a and ϕ_a .

show a contour plot of the total error in the estimation of the system's mass (in percent), for systems having a fixed SNR of 10 and using the AdvLigo noise. Fig. 4 shows a not monotonic trend for the error: for example, a system having $\eta = .25$ will have an error of about 1% if its mass is $4M_{\odot}$. As the mass increases, keeping η constant, (this is equivalent to scanning Fig. 4 from the lower right corner to the upper right one), there will be a local maximum of the error, due to the "island" on the right side of the plot, for $M \approx 55M_{\odot}$, where the error reaches about the 5%, then the error goes down for a while, and begins to grow again, from about $M = 100M_{\odot}$. On the other hand, if $\eta = 0.16$, as the system's mass increases it won't find any "island" of great error, and no local maxima will be present. We will recover this behavior later (Fig. 9).

We can use this kind of plots in another way. We calculate the ratio between the total variance (first plus second order) and the CRLB, and we let the SNR vary until the ratio goes under a chosen threshold for each point in the grid. Let us for example plot

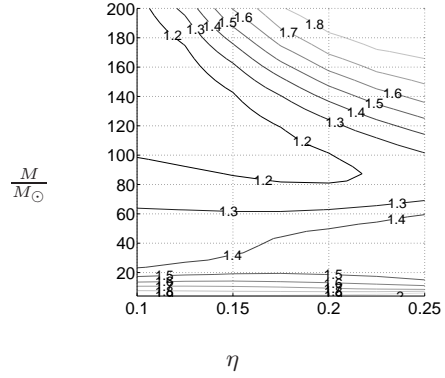


Figure 5. The ratio between the total mass error (first plus second order) and the CRLB, as a function of the total mass and symmetrized mass ratio. The systems have a fixed SNR, $\rho = 10$, and the AdvLigo noise is used.

$\frac{\sqrt{\sigma_{[1]_M}^2 + \sigma_{[2]_M}^2}}{\sigma_{[1]_M}}$ for $\rho = 10$, this is shown in Fig. 5. For highly symmetric massive systems the CRLB is nearly one half of the corrected error. If we want the ratio for the estimation of the total mass to be smaller than 1.05 for each value of M and η in the range considered, the SNR must be $\rho \geq 56.4$. We can perform the same kind of calculations for the other parameters. The biggest SNR we calculate in this way is the one required for the CRLB of the time parameter to attain a 5% precision, $\rho = 61.6$. Then we can say that for every binary system having mass and symmetric mass ratio in the range given above, a SNR of 61.6 assures that when using the CRLB for the errors' estimation our result will not differ more than 5% from the corrected errors.

It must be stressed that plots like those in Fig. 4 and Fig. 5 does not depend on the actual value of the arrival time and phase. The reason is the particular form of the signal, eq. (3.1), and the fact that t_a and ϕ_a are only contained linearly in the phase of the signal. Let us for example consider the (i, j) element of the CRLB, it depends on the real part of $h_i h_j^*$. Developing the derivations we have:

$$\begin{aligned} \Re[h_i h_j^*] &= \Re[(A_i + A(i\psi_i)) e^{i\psi} (A_j + A(-i\psi_j)) e^{-i\psi}] \\ &= A_i A_j + A^2 \psi_i \psi_j \end{aligned} \quad (4.2)$$

The arrival time and arrival phase will not be contained in terms like A or A_i , as the amplitude does not depend on them. Neither they will be in terms like ψ_a , because they were contained linearly in ψ . It is easy to see that the same kind of proof holds while calculating the $v...$, eqs. (2.8) to (2.18), and the optimal SNR, eq. (2.3).

As a general trend above SNR=20 the results are consistent with the results derived in [40] with both Monte Carlo simulations and the CRLB. Lower SNRs result in higher uncertainties, and occasionally the

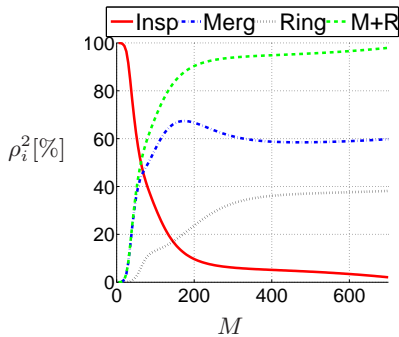


Figure 6. The relative contribution of the different phases to the total squared SNR for an equal mass system of total mass M

Monte Carlo simulations are below the CRLB. This behavior has already been observed in [37], for inspiral signals, where the author shows that the inconsistencies between Monte Carlo and CRLB are a consequence of the restriction $\eta < 0.25$ in the templates bank. By incorporating templates with $\eta > 0.25$, [37] obtains a good agreement between Monte Carlo and CRLB for $1.4 - 1.4$ and $5 - 5$ solar masses systems. However, discrepancies are still present in $10 - 10$ solar masses systems. The author acknowledges that there is not a satisfactory explanation for this inconsistency. More efforts must be made to fully understand how the boundary $\eta = 0.25$ affects Monte Carlo simulations and CRLB.

A comparison with our results that involves only the inspiral phase [22] indicates that by adding the merger and ringdown phases the errors decrease, but the necessary SNR (defined below) for the covariance to attain the CRLB can be up to a factor of two. For example looking at Fig. 8 of [22] 3 of the 4 rows are comparable (not the third one because in the IMR we use the total mass while in [22] the chirp mass). The SNR necessary to attain the CRLB in the IMR signals at $M_{\odot} = 20$ is between 9 and 11 while for inspiral phase waveforms is between 4 and 7. The absolute values of the errors are however larger for inspiral signals. In this case the contribution to the SNR of the inspiral phase is 99 percent (see for example Fig. 6 or its low M_{\odot} blow up in Fig. 7).

The bias does not play an important role, except for small SNRs (< 10) or for high mass systems, for which the error in the total mass and arrival phase is seriously affected by the bias. Unfortunately, while the use of the IMR allows for smaller values for the error estimation of the arrival time, total mass, and η , the same cannot be said of the arrival phase, for which the inclusion of the merger and ringdown phase seems to degrade the estimation, so that the error of the arrival phase estimation is in general higher than 2π , indicating that the arrival phase is unpredictable. In [44] the error for the arrival phase was estimated

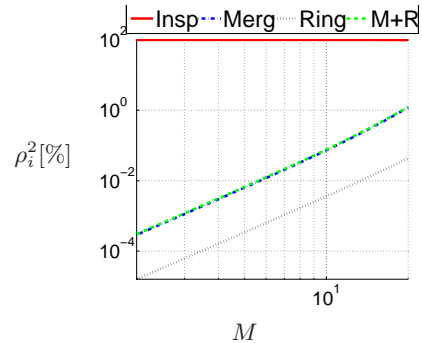


Figure 7. The relative contribution of the different phases to the total squared SNR (low mass detail)

using the inspiral 3.5 PN wave, obtaining a value of $\Delta\phi = 1.16 \text{ rad}$ for a system of $M = 20M_{\odot}$ at an SNR $\rho = 10$ using the AdvLigo noise. For the same system using the IMR wave we obtain $\Delta\phi = 14.8 \text{ rad}$ (9.98 rad considering the CRLB only). An estimation of the arrival phase error was not given in [40], and so a direct comparison is not possible. Since they are consistently above 2π , the errors on ϕ are not included in the plots. Let us stress that the large errors on the arrival phase does not imply that we cannot believe the estimations we have for the other parameters. The reason is that a correlation coefficient different from zero, say close to $+1$, tells us that an overestimation of the parameter x comes together with an overestimation of the parameter y ; but it doesn't tell anything about the relative magnitude of the errors. It is interesting to plot the errors values against the total mass of the system, for a fixed value of the SNR. Fig. 9 shows these plots for a mass range from $4M_{\odot}$ up to $500M_{\odot}$, and an SNR $\rho = 10$, using the AdvLigo noise. Fig. 10 does the same with the AdvVirgo noise. The inclusion of the second order variance and bias has visible consequences on the errors for large mass systems, for which the corrected error can be much larger than the CRLB. The plots show an oscillatory character of the bias, due mainly to the behavior of $b[2]$. For example we plot in Fig. 11 the bias orders on the total mass estimation against the system's mass, for $\eta = 0.2222$.

The second order covariance and the bias also seem to reinforce the minimum of the errors for $M 100M_{\odot}$. It is important to notice that a local minimum would be present also with the inspiral phase only. For example in Fig. 8 we show the error in the timing calculated for a $1.4-1.4 M_{\odot}$ binary system where only the inspiral phase is used (3.5 Post-Newtonian waveform, [44]), and a minimum is visible once the second order is included. To verify our new predictions in the errors for very large masses, numerical simulations or direct applications of parameter estimation pipelines are needed. Fig. 9 of [40] shows how BHs merger

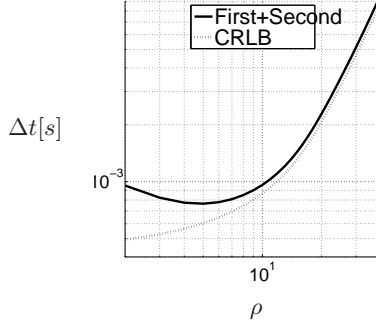


Figure 8. Minima in the error with respect to the mass can appear because of the contribution of the second order. In the plot the timing error is evaluated only for the inspiral signal of $\eta = 0.25$ at a fixed SNR, $\rho = 10$.

can have very high SNRs, even of 100, at 100 megaparsecs for advanced LIGO. At these SNRs our corrections would not be important. However, in order to have useful detection rates we would need to rely on sources up to a gigaparsec. In fact, in [45] a realistic rate for BH merger is given as 0.4 per million years in an equivalent Milky Way galaxy. Equation 5 in [45] also gives an approximation of the number of equivalent Milky way galaxies. Combining these two observations suggests that a realistic rate for BH mergers within a gigaparsec is about 1.6 per year.

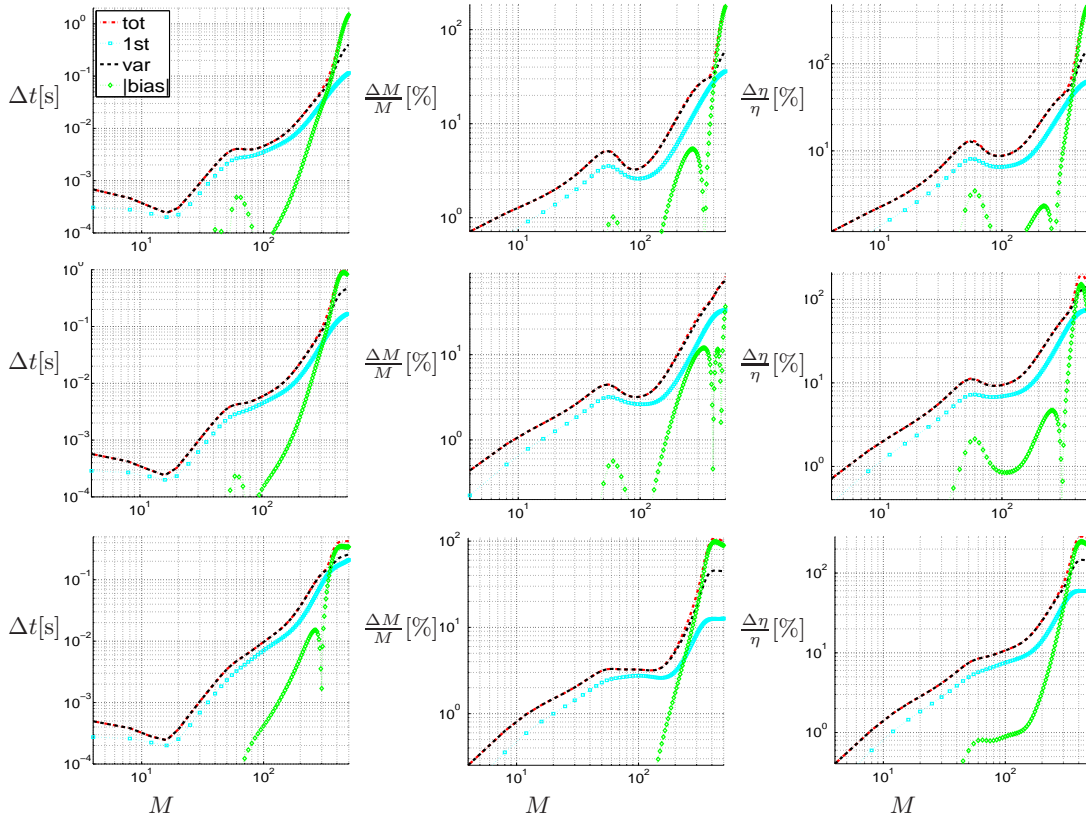


Figure 9. (Color Online) The errors plotted against the total mass, using the AdvLigo noise, for a fixed value of $\rho = 10$, and with $\eta = 0.25$ (top), $\eta = 0.2222$ (middle) and $\eta = 0.16$ (bottom). The “tot” dot-dashed line represents the MSE (variance plus bias); the “var” dashed line the variance (first plus second order); the dot-squares line is the first order variance (CRLB); the dot-diamonds line, finally, is the absolute value of the bias (first plus second order). The “tot” and “var” lines are nearly superimposed, except for very high masses

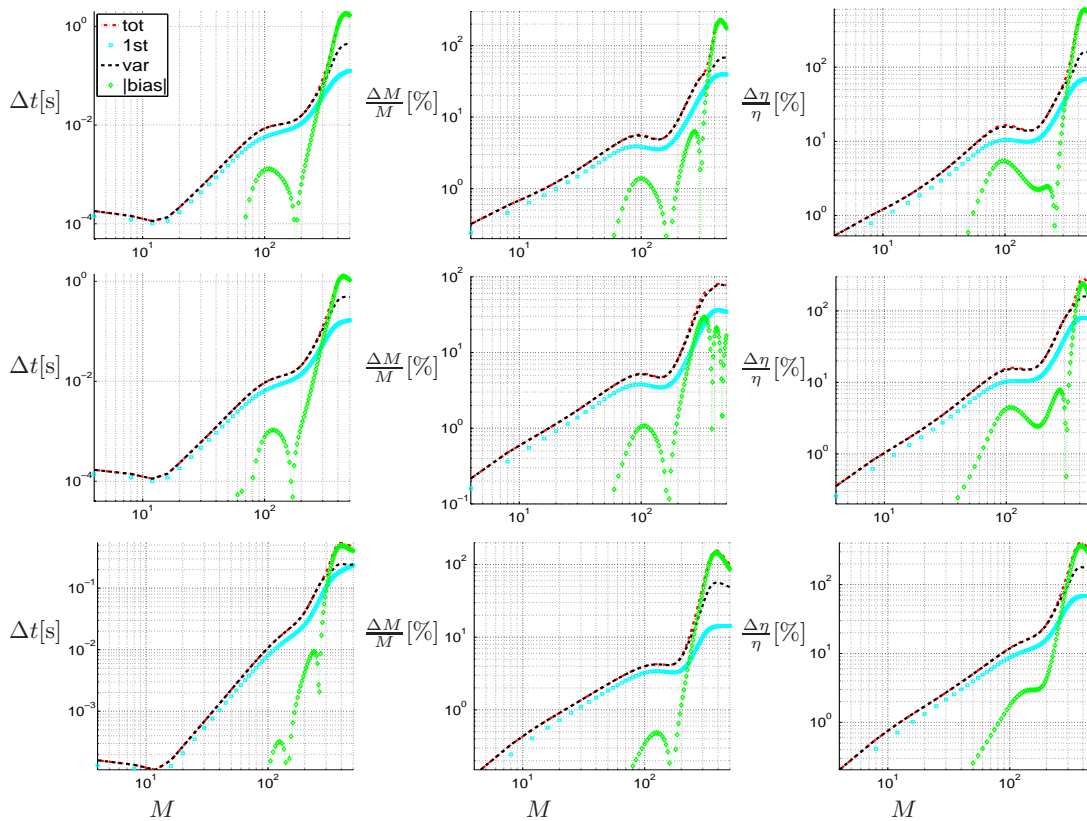


Figure 10. (Color Online) The same as fig. 9, except that the Advanced Virgo noise is used.

V. CONCLUSIONS AND FUTURE WORK

In this work we apply a recently derived methodology to the errors in estimating physical parameters from IMR signals. The asymptotic expansion of the bias and the covariance are critical to have realistic estimates of the error for SNR below 20 where the first detections of present and future laser interferometers might live. The behaviour of the errors, in terms of minima and maxima, in different regions of the parameter space appear to be more elaborate than predicted by the CRLB. For example the bias can become dominant for MLEs on systems with large masses. This paper will aid the preparatory work that the scientific community is undertaking to prepare for the scientific runs of the advanced version of the earth based laser interferometers.

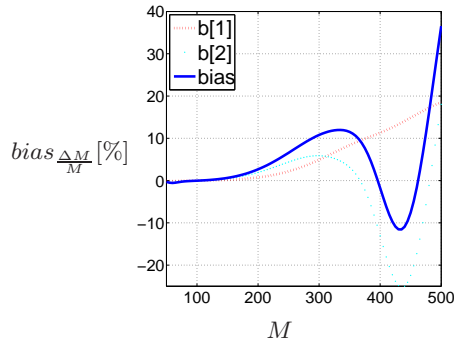


Figure 11. (Color Online) The bias, first order (red dashed), second order (cyan dotted) and total (blue line) using the Advanced LIGO noise, for a fixed value of $\rho = 10$, and with $\eta = 0.2222$

VI. ACKNOWLEDGMENTS

The authors would like to thank Alessandra Buonanno for discussions on the EOB waveforms. S.V.

thanks Walter Del Pozzo and Chris Van Den Broeck for useful discussions. M.Z. thanks the National Science Foundation for the support through the awards NSF855567 and NSF0919034.

-
- [1] LIGO Scientific Collaboration and Virgo Collaboration, *ArXiv*, gr-qc:1003.2480
- [2] <http://www.ligo.caltech.edu/advLIGO/>
- [3] <http://wwwcascina.virgo.infn.it/advirgo/>
- [4] R. Narayan, *New Journal of Physics*, **7**, 199 (2005).
- [5] J.Kormendy and D.Richstone, *Annu. Rev. Astron. Astrophys.*, **33**, 581 (1995).
- [6] R. Schodel et al., *Nature*, **419**, 694 (2002).
- [7] M.C. Miller and E.J.M. Colbert, *Int J. Mod. Phys. D*, **13**, 1 (2004).
- [8] S.Komossa et al., *Astrophys. J.*, **582**, L15 (2003)
- [9] L.Ballo et al, *Astrophys. J.*, **600**, 634 (2004)
- [10] M Guainazzi, E. Piconcelli, E. Jimenez-Bailon, and G. Matt, *Astron. Astrophys.*, **429**, L9 (2005)
- [11] D.A.Evans et al., *Arxiv*, astro-ph/0712.2669 (2007)
- [12] S.Bianchi, M. Chiaberge, E. Piconcelli, M. Guainazzi and G.Matt, *Arxiv*, astro-ph/0802.0825 (2008)
- [13] K.A. Postnov and L.R. Yungelson, *Living Rev.Relativity*, **9**, (2006)
- [14] P. Amaro-Seoane and M.Freitag, *Astrophys. J.*, **653**, L53 , astro-ph/0610478, (2006)
- [15] J.M. Fregeau, S.L. Larson, M.C. Miller, R.O'Shaughnessy, and F.A.Rasio, *Astrophys. J*, **646** ,L135 (2006)
- [16] I. Mandel, D.A. Brown, J.R. Gair, and M.C. Miller, *ArXiv*, astro-ph:0705.0285
- [17] A. Buonanno, Y. Pan, H.P. Pfeiffer, M.A. Scheel, L. Buchman and L.E. Kidder, *ArXiv*, gr-qc/0902.0790 (2009)
- [18] A. Buonanno, Y. Pan, J.G. Baker, J. Centrella, B.J. Kelly, S.T. McWilliams and R. Van Meter, *ArXiv* gr-qc/0706.3732 (2007)
- [19] T. Damour and A. Nagar, *ArXiv* gr-qc/0902.0136 (2009)
- [20] L. Santamaria, F. Ohme, P. Ajith, B. Bruegmann, N. Dorband, M. Hannam, S. Husa, P. Moesta, D. Pollney, C. Reisswig, E.L. Robinson, J. Seiler and B. Krishnan, *ArXiv* gr-qc/1005.3306 (2010)
- [21] The ninja collaboration: <https://www.ninja-project.org/doku.php>
- [22] M. Zanolin, S. Vitale and N. Makris, *Phys. Rev. D*, **81** 124048 (2010)
- [23] C.W. Helstrom, *Statistical Theory of Signal Detection*, International Series of Monographs in Electronics and Instrumentation, **vol. 9**, (Pergamon Press, Oxford; New York, 1968), 2nd edition.
- [24] L. Blanchet, *Living Rev. Relativity*, **9** (2006)
- [25] F. Pretorius, *Phys. Rev. Lett.* **95**, 121101 (2005)
- [26] M. Campanelli, C.O. Lousto, P. Marronetti, and Y. Zlochower, *Phys. Rev. Lett.* **96** 111101 (2006).
- [27] J.G. Baker, J. Centrella, D.I. Choi. M. Koppitz and J. van Meter, *Phys. Rev. Lett.* **96** 111102 (2006)
- [28] F. Herrmann, I. Hindler, D. Shoemaker and P. Laguna, *Class. Quantum Grav.*, **24**, S33 (2007)
- [29] U. Sperhake, *ArXiv*: gr-qc/0606079
- [30] B. Brügmann, J.A. González, M. Hannam, S. Husa, U Sperhake and W. Tichy, *ArXiv*:gr-qc/0610128 (2006)
- [31] T. Thornburg, P. Diener, D. Pollney, L. Rezzola, E. Schnetter, E. Seidel and R. Takahashi, *Class. Quantum Grav.* **24** 3911 (2007)
- [32] Z.B. Etienne, J.A. Faber, Y.T. Liu, S.L. Shapiro and T.W. Baumgarte, *ArXiv*:gr-qc/0707.2083 (2007)
- [33] B.S. Sathyaprakash and B.F. Schutz, *Living Rev.Relativity*, **12** (2009)
- [34] D. Nicholson, A. Vecchio, *Phys. Rev. D* **57**, 4588 (1998)
- [35] R. Balasubramanian, B.S. Sathyaprakash and S.V. Dhurandhar, *Phys. Rev. D* **53**, 3033 (1996)
- [36] R. Balasubramanian and S.V. Dhurandhar, *Phys. Rev. D*, **57**, 3408 (1998)
- [37] T. Cokelaer, *Class. Quantum Grav.* **25**, 184007 (2008)
- [38] P. Ajith et al., *Class. Quantum Grav.*, **24**, S689 (2007)
- [39] P. Ajith, *Class. Quantum Grav.*, **25**, 114033 (2008)
- [40] P. Ajith and S. Bose, *arXiv*, gr-qc/0901.4936 (2009)
- [41] P. Ajith et al., *ArXiv*, gr-qc/0710.2335
- [42] P. Ajith, M. Hannam, S. Husa, Y. Chen, B. Brügmann, N. Dorband, D. Müller, F. Ohme, D. Pollney, C. Reisswig, L. Santamaria and J Seiler, *arXiv*, gr-qc/0909.2867v1 (2009)
- [43] C. Cutler and E.E. Flanagan, *Phys. Rev. D*, **49**, 6, 2658 (1994)
- [44] K.G Arun, B.R. Iyer, B.S. Sathyaprakash and P.A. Sundararajan, *arXiv*, gr-qc/0411146 (2005)
- [45] J. Abadie et al, *Class. Quantum Grav.*, **27**, 173001 (2010)